

Sb (III) Removal from Aqueous Solutions by the Mesoporous Fe₃O₄/GO Nanocomposites: Modeling and Optimization Using Artificial Intelligence

X. L. Wu¹, R. S. Cao¹, J. W. Hu^{1,2,*}, C. Zhou¹, and X. H. Wei³

¹ Guizhou Provincial Key Laboratory for Information Systems of Mountainous Areas and Protection of Ecological Environment, Guizhou Normal University, Guiyang, Guizhou 550001, China

² Cultivation Base of Guizhou National Key Laboratory of Mountainous Karst Eco-environment, Institute of Karst, Guizhou Normal University, Guiyang, Guizhou 550001, China

³ Department of Applied Chemistry, College of Chemistry and Molecular Engineering, Peking University, Beijing 100871, China

Received 20 June 2018; revised 06 November 2020; accepted 27 June 2021; published online 15 May 2023

ABSTRACT. The mesoporous graphene oxide-supported ferroferric oxide (Fe₃O₄/GO) nanocomposites (the average size of 30.08 nm) were controllably synthesized in the present study. The successful in situ growth of Fe₃O₄ nanoparticles on GO surface was ascribed to the oxygen-containing groups on GO. The magnetic separation was employed for Sb(III) removal from aqueous solutions and artificial intelligence techniques were adopted to reduce the number and cost of experiments, in order to render these nanocomposites of a practical value. The three methods, including response surface methodology (RSM), artificial neural network-genetic algorithm (ANN-GA) and artificial neural network-particle swarm optimization (ANN-PSO), were used to model and optimize the removal of Sb(III) from aqueous solutions. These three models were evaluated based on correlation coefficient (R^2) and mean squared error (MSE). The higher R^2 value and lower MSE of ANN-GA demonstrated the superiority of ANN-GA model over ANN-PSO and RSM models. Analysis of variance, gradient boosted regression trees (GBRT) and Garson method exhibited that contact time was the most influential variable for the Sb(III) removal. Fitting of isotherm data showed that the removal process was controlled by the monolayer adsorption on a homogeneous surface based on the values of R^2 , x^2 , sum of absolute errors (SAE) and average percentage errors (APE). The adsorption process followed the pseudo-second-order model, which was spontaneous and entropy-driven. It was observed that the adsorption process was accompanied with the redox reaction based on the XPS analysis. The regeneration experiments showed that the mesoporous Fe₃O₄/GO nanocomposites are an effective and reusable adsorbent within four regeneration cycles.

Keywords: graphene oxide-supported ferroferric oxide, Sb(III), artificial intelligence, isotherm study, kinetic study, thermodynamic study

1. Introduction

There has been a growing concern for the negative effect of antimony (Sb) on human health due to its increase in industrial and agricultural uses. Sb is a toxic heavy metal widely used in a variety of industrial products, such as fire retardants, batteries, cosmetics, cable covering, pigments, ceramics, and glass (Filella et al., 2007). Sb and its compounds have been listed as a priority pollutant by United States Environmental Protection Agency (US EPA) and European Union (EU) with the maximum permissible concentrations of 6 and 10 µg/L for Sb in drinking water, respectively (Shan et al., 2014). It has also been registered as a concern pollutant by the Environmental Protection Department of Japan with the maximum permissible value of 2 µg/L (Kappen et al., 2017). For both the standards of China and World Health Organization, the maximum permissible concentration of Sb is 5 µg/L in drinking water. High concentrations of Sb were

detected in soils of shooting ranges, mining fields, and smelter industrial sites (Rakshit et al., 2011).

China has the largest reserve and production capacity of antimony in the world. Xikuangshan is the main production area in Hunan province, which is called the World Antimony Capital (Guo et al., 2009). The Sb pollution in this region has caused a tremendous concern because the long-term mining activities have destroyed the ecological environment in this area. The Sb concentration around the mining area was reported ranging from 100.60 to 5045.00 mg/kg in soil samples and over 7,000.00 µg/L in wastewater samples (Guo et al., 2009). Sb predominately exists in inorganic forms of Sb(III) and Sb(V) in the natural environment. However, the toxicity of Sb(III) is considered 10.00 times greater than that of Sb(V) (Krachler et al., 2001). Therefore, it is necessary to develop feasible and eco-friendly means to eliminates Sb(III) from rivers and streams.

Different materials such as bentonite (Xi et al., 2011), diatomite (Sarı et al., 2010), activated carbon (Navarro et al., 2002), and iron-based materials (Watkins et al., 2006) have previously been employed to remove Sb(III) from wastewater. Since iron-based materials were strongly magnetic, they have

* Corresponding author. Tel.: +86-851-86702710.

E-mail address: jw.hu@gznu.edu.cn (J. W. Hu).

ISSN: 1726-2135 print/1684-8799 online

© 2023 ISEIS All rights reserved. doi:10.3808/jei.202300495.

been considered as an effective and facile method for separating magnetic particles from solid-liquid mixtures (Qi et al. 2015). In general, magnetic nanocomposites are usually of high sorption efficiency, sorption capacity, and selectivity for radionuclides and heavy metal ions. Previous studies have reported that the synthesized Fe_3O_4 nanoparticles as a promising absorbent have been used for heavy metals elimination from wastewater due to their large specific surface area, extremely the small particle size (Satyabrata et al., 2004; Shen et al., 2009; Cao et al., 2017). However, there are still some technical problems in practical applications for Fe_3O_4 nanoparticles (e.g., agglomeration, poor stability, shortage of durability and mechanical strength), which limit their use in other areas (Cao et al., 2017).

Graphene consists of extraordinarily hexagonal sp^2 carbon network with a two-dimensional honeycomb lattice structure and possesses many superb characteristics such as high thermal conductivity, large surface area, and remarkably optical, electrical and mechanical properties (Chung et al., 2013; Chang et al., 2014). Generally, graphene is easily exfoliated and oxidized by strong oxidants leading to the formation of graphene oxide (GO). Due to the huge specific surface area ($2,630 \text{ m}^2/\text{g}$), GO has been widely applied in water treatment (Li et al., 2014). The prepared graphene oxide-supported ferroferric oxide ($\text{Fe}_3\text{O}_4/\text{GO}$) nanocomposites for effective pollutants removal have demonstrated a strong affinity and reversibility for a range of pollutants (Jiao et al., 2015). $\text{Fe}_3\text{O}_4/\text{GO}$ nanocomposites have attracted a tremendous attention among researchers and widely applied in many areas, e.g., immobilization of bioactive substances, energy storage, and environmental remediation (Namvari and Namazi, 2014; Guo et al., 2015; Thirugnanasambandham and Sivakumar, 2015). Considering its superior characteristics, especially convenient separation with an external magnetic fields, $\text{Fe}_3\text{O}_4/\text{GO}$ nanocomposites are regarded as a potential adsorbent for the removal of organic/inorganic contaminants, heavy metal ions and radionuclides from the large volumes of aqueous solutions. Yang et al. (2017) examined Sb(III) removal by $\text{Fe}_3\text{O}_4/\text{GO}$ nanocomposites and found that the specific magnetism was up to 87.3 emu/g and the maximum adsorption capacity was 9.59 mg/g at $\text{pH} = 3.0 \sim 9.0$. However, this study did not involve the size and pore of Fe_3O_4 nanoparticles and optimize the process of the removal of Sb(III) from aqueous solutions.

Response surface methodology is a collection of mathematical and statistical techniques based on the fit of a polynomial equation to the experimental data, which can describe the behavior of a data set with the objective of making statistical provisions (Hanrahan et al., 2007; Zhang et al., 2010; Chaves et al., 2015). It can be well applied when a response or a set of responses of interest are influenced by several variables (Kirmizakis et al., 2014; Thirugnanasambandham and Sivakumar, 2015). The objective is to simultaneously optimize the levels of these variables to attain the best system performance. AI has recently gained an enormous development because it has been widely applied in various fields, e.g., big data, human-computer games, robotics, image understanding, automatic programming, autonomous driving, pattern recognition, and intelligent internet search (Ogiela and Tadeusiewicz, 2003; Pedrycz et al., 2015). Artificial neural network (ANN), one of the AI primary tools,

was biologically inspired computer program to simulate the means in which the human brain processes information (Zhang and Pan, 2014). Genetic algorithm (GA) is a randomized parallel search algorithm based on the evolutionary principles and chromosomal processing in natural genetics, which has been applied to optimization problems (Karimi and Ghaedi, 2014). ANN combined with GA has been successfully used to model and optimize the removal processes for pollutants from wastewater, viz., dyes, heavy metals, and phosphate (Fan et al., 2017, 2018; Ruan et al., 2018). There are some characteristics (e.g., reliability, robustness, and salient topological features) in capturing the non-linear relationships of variables in complex systems (Abdollahi et al., 2013). In addition, particle swarm optimization (PSO) inspired by social behavior of bird flocking or fish schooling. The system is initialized with a population of random solutions and searches for optima by updating velocity and position (Toushmalani, 2013). ANN-PSO also has been employed to model and optimize the processes of removing pollutants from aqueous solutions.

Hitherto, the previous studies have reported that several nanomaterials were used to remove pollutants from the environment (Chen et al., 2014a, 2014b; Cao et al., 2017; Fan et al., 2017; Ruan et al., 2018). However, some of these studies discussed only from the perspective of engineering applications (Cheng et al., 2018; Dong et al., 2018; Maamoun et al., 2020), while the others made investigation merely into the mechanism (Behnam et al., 2019; Chen et al., 2019; Zhou et al., 2019). The preliminary mechanism and cost reduction should be taken into account simultaneously in these studies. Hence, the objective of the present study was to controllably synthesize the $\text{Fe}_3\text{O}_4/\text{GO}$ nanocomposites by coprecipitation method and characterize them using X-ray diffraction (XRD), scanning electron microscopy (SEM), X-ray photoelectron spectroscopy (XPS), transmission electron microscope (TEM), and superconducting quantum interference device (SQUID). In the present study, the AI (ANN-GA, ANN-PSO) and RSM models were developed to optimize the removal of Sb(III) from water solutions using the $\text{Fe}_3\text{O}_4/\text{GO}$ nanocomposites by considering different operational parameters, i.e., operating temperature, initial pH, contact time and initial Sb(III) concentration. First, the $\text{Fe}_3\text{O}_4/\text{GO}$ nanocomposites were controllably synthesized by coprecipitation method and characterized using X-ray diffraction (XRD), scanning electron microscopy (SEM), X-ray photoelectron spectroscopy (XPS), transmission electron microscope (TEM), and superconducting quantum interference device (SQUID). The adsorption/desorption isotherms and BJH pore-size distribution curves were utilized to identify the mesoporous structures of the $\text{Fe}_3\text{O}_4/\text{GO}$ nanocomposites. Then, batch experiments were designed according to 4-factor-3-level of Box-Behnken design (BBD) model of RSM. The RSM and AI (ANN-GA, ANN-PSO) models were developed to optimize the removal of Sb(III) from aqueous solutions using the $\text{Fe}_3\text{O}_4/\text{GO}$ nanocomposites by considering different operational parameters, i.e., operating temperature, initial pH, contact time, and initial Sb(III) concentration. Feed forward back-propagation artificial neural networks (BP-ANN) was trained by the data set obtained from RSM, and the trained model was used for predicting the maximum removal efficiency of

Sb(III). Analysis of variance, gradient boosted regression trees (GBRT) and Garson methods were used to explore the importance of the factors. Finally, the Langmuir, Freundlich and Temkin models were utilized for analysis of the adsorption equilibrium, and the better model was selected by comparing the R^2 value, Chi-square test (χ^2), the sum of absolute errors (SAE) and average percentage errors (APE). Kinetic (pseudo-first-order, pseudo-second-order, and intraparticle diffusion) and thermodynamic studies (Van't Hoff equation) were carried out to reveal the potential mechanisms of adsorption process. In addition, the effectiveness and reusability of Fe₃O₄/GO nanocomposites were evaluated by the regeneration experiments.

2. Materials and Methods

2.1. Materials

All chemicals (i.e., K(SbO)C₄H₄O₆·1/2, FeCl₃·6H₂O, FeCl₂·4H₂O, NaOH, and HCl) used in this study were of analytical grade, and all solutions were prepared using deionized water. The graphite powder (the size of particle < 30 μm, purity > 99.85%) was purchased from Sinopharm Chemical Reagent. The Sb(III) stock solution (1,000 mg/L) was prepared by dissolving an amount of K₂SbC₄H₄O₇ in deionized water.

2.2. Preparation of the GO and Fe₃O₄/GO Nanocomposites

GO was synthesized using the modified Hummers method in the present work (Vimlesh et al., 2010). Fe₃O₄/GO nanocomposites were prepared by coprecipitation method (Cao et al., 2017). The successful in situ growth of Fe₃O₄ nanoparticles on GO surface during the synthetic process of Fe₃O₄/GO nanocomposites was ascribed to the oxygen-containing groups of GO (Yang et al., 2017). The as-synthesized composites in this study do not only have the excellent adsorption properties of GO, but also possess the superparamagnetism of Fe₃O₄ nanoparticles. Therefore, the proportion of Fe₃O₄ to GO was optimized during the preparation of composites to take advantage of the strong adsorption properties of GO and the magnetism of Fe₃O₄.

GO (300 mg) was dispersed into deionized water (100 mL) by ultrasonication for 1 h. 10 mL solution of FeCl₃·6H₂O (2.7030 g) and FeCl₂·4H₂O (1.9881 g) in deionized water was added to the GO suspension at room temperature and the process was purged with N₂ for 30 min. Then the temperature was raised to 85 °C and a 30% ammonia solution was added to pH = 10.0. After being rapidly stirred for 1h, the suspension was cooled to room temperature. The resulted black precipitate was centrifuged at 4,500 rpm for 10 min and washed three times with deionized water and finally dried in a vacuum oven at 60 °C for overnight to yield the Fe₃O₄/GO nanocomposites.

2.3. Characterization of As-Prepared Fe₃O₄/GO Nanocomposites

The Fe₃O₄/GO nanocomposites were examined on an XRD instrument for phase identification using the LynxEye array detector with a Cu-Kα X-ray source (generator tension = 40 kV, current = 40 mA, Bruker Corporation, Karlsruhe, Germany). The

morphology was examined using TEM images (TecnaiG2 F20, FEI Co., Ltd., Hillsboro, OR, USA). XPS measurements were recorded on an ESCALAB 250Xi spectrometer using monochromatized Al-Kα radiation (hν = 1,486.6 eV), all binding energies were calibrated by using the contaminant carbon (C_{1s} = 284.8 eV) as a reference (Thermo Electron Corporation, Waltham, MA, USA). FTIR measurement used a Nicolet 6700 spectrometer (Nicolet Instrument Corporation, Madison, WI, USA). Magnetization measurements were carried out using a SQUID magnetometer (MPMS XL-7, Quantum Design, Inc., San Diego, CA, USA) under applied magnetic field at room temperature. Brunner-Emmet-Teller (BET) surface areas of the Fe₃O₄/GO composites were obtained from N₂ adsorption isotherms at 77 K with a micromeritics 3 Flex surface characterization analyzer (outgass time: 3.0 h, outgass temperature: 300.0 °C, Micromeritics Instrument Corporation, Norcross, GA, USA).

2.4. Adsorption Experiments

1,000 mg/L of Sb(III) stock solution was diluted into 30, 50, and 70 mg/L using deionized water, respectively. 30 mg of Fe₃O₄/GO nanocomposites was added in 50 mL of Sb(III) solution (30, 50, and 70 mg/L). At the same time, the initial pH of mixture was adjusted to the expected value by using 0.1 mol/L HCl or 0.1 mol/L NaOH. The mixture was shaken in a vibrator (HZQ-F160, HDL) at 200 rpm. Finally, the Fe₃O₄/GO nanocomposites were separated from the mixture by magnet after the end of reaction. The factors including initial Sb(III) concentration, initial pH, contact time, and operating temperature on the removal efficiency of Sb(III) were investigated using the batch adsorption experiments (single factor experiments). The Sb(III) concentration for the sample solutions was determined using an inductively coupled plasma optical emission spectrometry (optima 5,300 V). The 20% experiments (the replication experiments) were randomly selected in all experiments and the average values of results were used for data analysis. The removal rate of Sb(III) from the sample solution was calculated from Equation (1):

$$P = \frac{(C_0 - C_t) \times 100}{C_0} \quad (1)$$

where P is the removal rate of Sb(III), C_t is the concentration of Sb(III) after removal and C_0 is the initial Sb(III) concentration (mg/L). The removal capacity (q_e) of Sb(III) from the sample solution was calculated using the following Equation (2):

$$q_e = \frac{(C_0 - C_t) \times v}{m} \quad (2)$$

where q_e is the removal capacity of Sb(III) from the sample solution (mg/g), v is the volume of the solution used (mL), and m is the quality of Fe₃O₄/GO nanocomposites used (mg).

2.5. RSM Used for Experimental Design

The experimental design mainly referred to the previous studies and the levels of different factors in removal process were

determined by single factor experiments (Table S1). According to BBD, each independent variable is set at one of three equally spaced values, usually coded as -1 , 0 , and $+1$. For contact time, 50, 60, and 70 min were selected as minimum “ -1 ”, middle “ 0 ”, and maximum “ $+1$ ”, respectively. The suitable levels of contact time and initial Sb(III) concentration should be determined in the single factor experiments. The adsorption of Sb(III) onto the $\text{Fe}_3\text{O}_4/\text{GO}$ was examined at different initial Sb(III) concentrations ranging from 1 to 70 mg/L with a pH of 7, a contact time of 60 min and a temperature of 25 °C. It was found that the Sb(III) removal efficiency was decreased with the higher initial Sb(III) concentration and reached 82.79% at 50 mg/L with the other conditions being equal. According to BBD, 50 mg/L was set as the centre point, and 30 and 70 mg/L were considered as the lower and upper limits, respectively, since a range of concentration effected on removal efficiency should be observed. Effect of different contact times (2 ~ 100 min) on Sb(III) adsorption was investigated with a temperature of 25 °C, a pH of 7 and an initial Sb(III) concentration of 30 mg/L. It was demonstrated that the Sb(III) removal efficiency was raised with the longer reaction time and attained with 80.12% under a contact time of 50 min with the other conditions being equal. The Sb(III) removal efficiency reached more than 80% under a contact time of $\text{Fe}_3\text{O}_4/\text{GO}$ (50 ~ 60 min) and an initial Sb(III) concentration of $\text{Fe}_3\text{O}_4/\text{GO}$ (30 ~ 50 mg/L) at a pH of 7 at a temperature of 25 °C.

2.6. ANN-GA and ANN-PSO Used for Optimizing Parameters

The methods of ANN-GA and ANN-PSO were described in our previously published study (Cao et al., 2017). In this study, a slight revision was made on these methods, and the flow charts of ANN-GA and ANN-PSO are shown in Figures S1 and S2, respectively (Chen et al., 2017; Wang et al., 2017).

2.7. Adsorption Equilibrium Study

The Langmuir, Freundlich and Temkin adsorption models were employed to study the mechanism and properties of $\text{Fe}_3\text{O}_4/\text{GO}$ nanocomposites for the Sb(III) removal from aqueous solutions. The specify equations and descriptions can be found in supplementary data of this studies (Table S2).

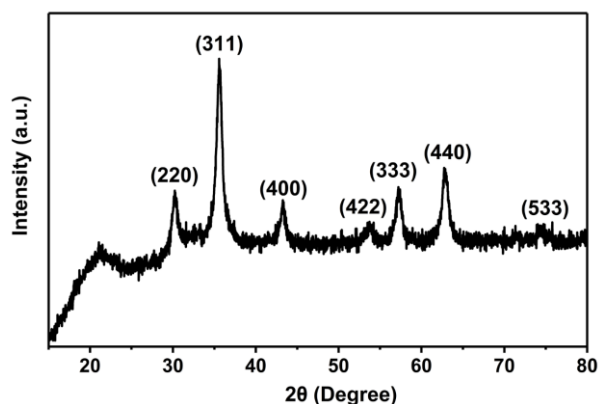


Figure 1. XRD pattern of $\text{Fe}_3\text{O}_4/\text{GO}$.

2.8. Sensitivity Analysis

Sensitivity analysis was carried out to explore the connection weights of the trained ANN, which referred to our published study (Cao et al., 2017). GBRT, also as an AI tool, is a flexible non-parametric statistical learning technique for classification and regression, revealing the feature importance via heuristic algorithm (Persson et al., 2017).

3. Results and Discussion

3.1. Characterization of the $\text{Fe}_3\text{O}_4/\text{GO}$ Composites

3.1.1. XRD and TEM

The morphology and structure of the nanocomposites were analyzed by XRD and TEM. As shown in the Figure 1, the XRD pattern of GO shows that the peak at 10.9° is due to the (002) crystalline plane of GO. It is displayed that seven distinct diffraction peaks of full width at half maximum are identified for 2θ at 30.1, 35.4, 43.1, 53.2, 56.0, 62.7, and 74.0° , respectively. These diffraction peaks correspond to the crystalline plane of Fe_3O_4 are (220), (311), (400), (422), (333), (440), and (533), respectively. In Figure 2, the TEM image of the $\text{Fe}_3\text{O}_4/\text{GO}$ nanocomposites shows that the nanocomposites were well-dispersed on the surface of the GO. It is demonstrated that Fe_3O_4 was successfully supported on the GO. In addition, $\text{Fe}_3\text{O}_4/\text{GO}$ nanocomposites were successfully prepared because the formed coordination compounds (Fe^{3+} and Fe^{2+} in solution reacted with the carboxyl functional groups of GO) were easily deposited on the GO sheets under alkaline condition. The following reaction mechanism of Fe_3O_4 supported on the GO in alkaline solution (Teo et al., 2012; Yang et al., 2017) was previously confirmed:

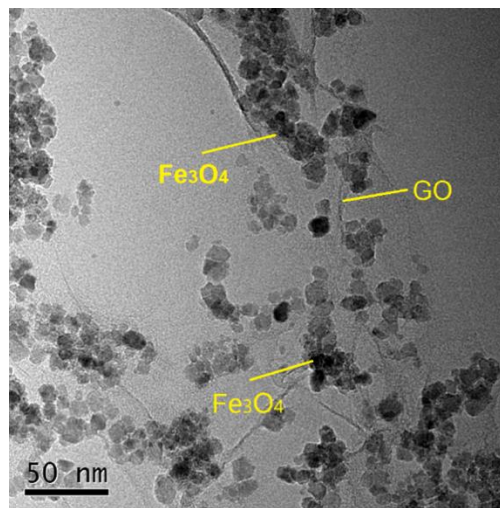
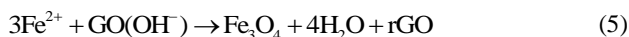
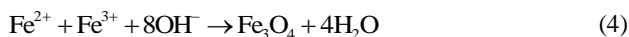


Figure 2. TEM image of $\text{Fe}_3\text{O}_4/\text{GO}$.

3.1.2. SEM and FT-IR

The Fe_3O_4 nanoparticles are uniformly distributed on the GO as shown in SEM image (Figure 3). According to our statistical analysis, the maximum, minimum, and average sizes of Fe_3O_4 nanoparticles were 57.88, 13.24, and 30.04 nm, respectively. The detailed information concerning the size distribution of $\text{Fe}_3\text{O}_4/\text{GO}$ is illustrated in Table S3 and Figure S3. Cao et al. (2017) reported that the average size of Fe_3O_4 nanoparticles of $\text{Fe}_3\text{O}_4/\text{rGO}$ composites were 300 nm using hydro-thermal method. Zhu et al. (2017) found that the size distribution of Fe_3O_4 particles was 250 ~ 350 nm also by hydro-thermal method. It was proven that the average size of prepared Fe_3O_4 particles using coprecipitation method in this study was far smaller than that of Fe_3O_4 particles made by hydro-thermal method. Zong et al. (2013) indicated that the average size of Fe_3O_4 particles was 20 nm using the coprecipitation method. Therefore, the Fe_3O_4 nanoparticles were controllably synthesized in this study. Amines are typically used as cosurfactant, which can lead to iron oxide nanoparticles obtained with a narrow size and strong magnetism. This was the reason why Fe_3O_4 particles possess a small size in this work. Additionally, the oxygen vacancy may be the main reason for causing the difference between varied morphologies.

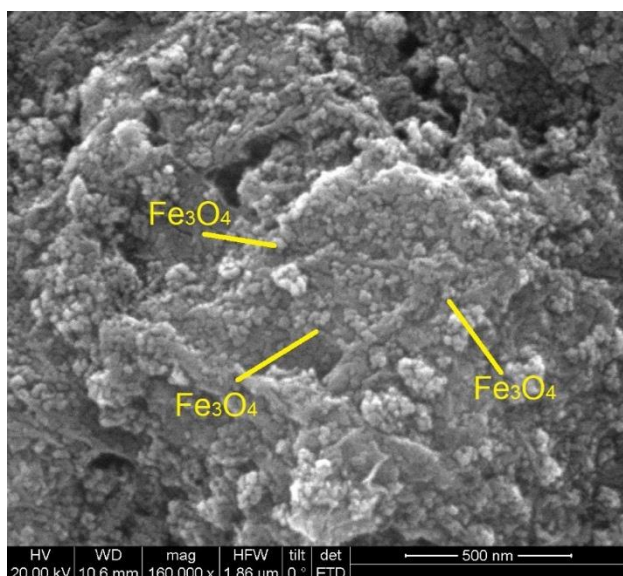


Figure 3. SEM image of the $\text{Fe}_3\text{O}_4/\text{GO}$.

The characteristic absorption peaks for Fe–O bond appeared at 570 and 468 cm^{-1} in FT-IR spectrum of the $\text{Fe}_3\text{O}_4/\text{GO}$ nanocomposites (Figure 4). The characteristic absorption peaks at 3,438, 1,633, and 1,120 cm^{-1} were related to the vibration absorption peak of –OH, C=O in carboxyl and C–O–C, respectively. It was thus confirmed that a great number of oxygen-containing groups exist on the surface of the GO and Fe_3O_4 .

3.1.3. Superconducting Quantum Interference Device

The hysteresis loop of the $\text{Fe}_3\text{O}_4/\text{GO}$ nanocomposites is shown in Figure 5. The materials can be facilely separated in solid-liquid phase by a magnet owing to the strong magnetism

of the materials up to 67.1 emu/g. The $\text{Fe}_3\text{O}_4/\text{GO}$ nanocomposites belong to soft magnetism since the surplus magnetic strength and magnetic coercive force were approximately of zero value. The hysteresis loop of $\text{Fe}_3\text{O}_4/\text{GO}$ is close to “S”, demonstrating its superparamagnetism.

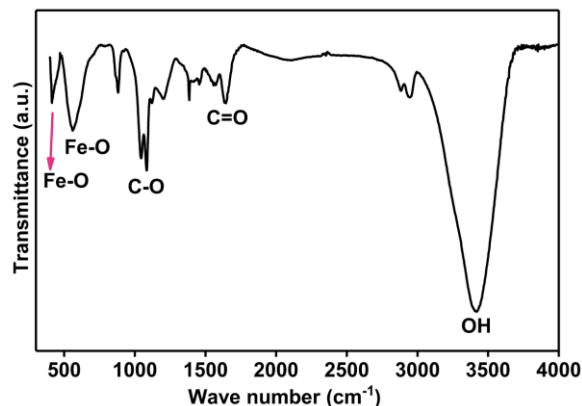


Figure 4. FTIR spectrum of the $\text{Fe}_3\text{O}_4/\text{GO}$.

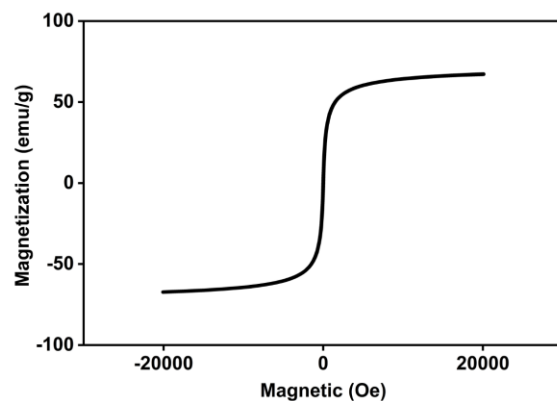


Figure 5. Magnetization hysteresis loop of the $\text{Fe}_3\text{O}_4/\text{GO}$ nanocomposites at room temperature.

3.1.4. Pore Size Studies

The isotherms of $\text{Fe}_3\text{O}_4/\text{GO}$ nanocomposites illustrate a type of IV curve, which represents the mesopore (Figure 6a). A loop at relative pressure between 0.43 and 0.99 is observed, indicating the pore size distribution in the mesoporous region. The BET specific surface area of the $\text{Fe}_3\text{O}_4/\text{GO}$ nanocomposites was 160.25 m^2/g . Further, the pore size distribution curves in Figure 6b show that $\text{Fe}_3\text{O}_4/\text{GO}$ nanocomposites possess one kind of mesopores with the size centered at 3.65 nm. The process of mesoporous materials prepared was affected by some factors, e.g., surfactants, inorganic species, concentration, pH, contact time and temperature (Allothman, 2012). The mesoporous materials have some features, e.g., uniform pore size ranging from 2 to 50 nm and high specific surface area, which were widely employed in energy conversion and storage, biomedicine and environmental remediation. In the preparation process, inorganic species interact with surfactants driven by coulomb force, covalent bond or hydrogen bonding.

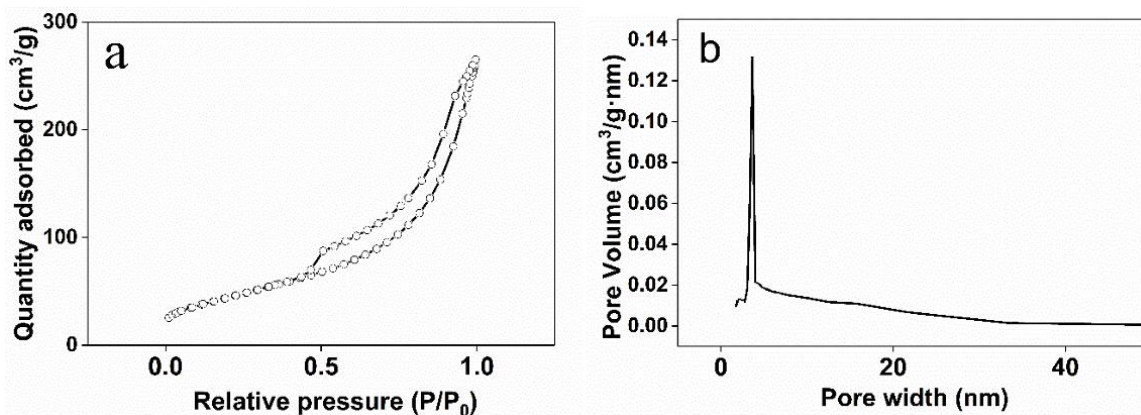


Figure 6. (a) Adsorption/desorption isotherms of the $\text{Fe}_3\text{O}_4/\text{GO}$ nanocomposites and (b) BJH pore-size distribution curves of the $\text{Fe}_3\text{O}_4/\text{GO}$ nanocomposites.

3.2. RSM Modeling and Prediction

The experimental design matrix and the response using BBD are shown in Table S4. Final equation in terms of coded factors for response is given below (Equation (6)):

$$\begin{aligned}
 F = & 62.85 + 30.36A - 0.71B - 0.51C - 0.30D \\
 & - 0.09AB + 0.22AC + 0.13AD + 0.12BC \\
 & - 6.74 \times 10^{-3}BD - 3.73 \times 10^{-3}CD - 2.43A^2 \\
 & - 8.63B^2 - 0.06C^2 - 2.98 \times 10^{-3}D^2
 \end{aligned} \quad (6)$$

The predicted values of the response were calculated using the above mentioned equation. The positive and negative symbols of the coefficients in this equation represent a synergistic effect and an antagonistic effect, respectively. From the equation, the constant is 62.85, which was not affected by any factor or interaction of the factors. It was shown that the linear terms (B , C , and D), the interaction term (AB) and the second-order terms (A^2 , B^2 , C^2 , and D^2) have a negative effect on the response. In contrast, the linear term (A) and the interaction terms (AB , AC , and AD) illustrated a positive influence on the response. This means that there would be an increase in the efficiency of Sb(III) removal with an increase in the value of these parameters.

The analysis of variance (ANOVA) for Sb(III) removal of aqueous solutions based on BBD gives the F -value, p -value, coefficient of determination (R^2) and the corresponding results (Table 1), which are used to verify the fitness and significance of the model. Since the p -value (0.0024) is less than 0.0500 and the “lack of fit” (0.1053) is not significant, the model is considered to be significant. The R^2 value of the model was 0.8334, and this means that the model has a high significance. The signal to noise ratio was tested by the “adequate precision”, and the value greater than or equal to 4 should be satisfied. Obviously, the value of signal to noise ratio was greater than 4 in this study, which satisfies the model requirements. In addition, a lower value of the coefficient of variation ($CV = 6.17\%$) demonstrates a good precision and reliability for the model. The optimum predicted for the maximum removal of Sb(III) by $\text{Fe}_3\text{O}_4/\text{GO}$ nanocomposites was approximately 90.12%, and the corre-

sponding optimal parameters of removal process are as follows: Temperature = 30.00 °C, contact time = 70.00 min, initial pH = 7.06, and initial Sb(III) concentration = 30 mg/L.

From Figure S4, most of the data points were distributed near the straight line, demonstrating an excellent relationship between the experimental and predicted values of the response. In addition, the interaction effect of process variables on response is further demonstrated by contour and 3D response surface plots (Figure 7) for the removal of Sb(III) by $\text{Fe}_3\text{O}_4/\text{GO}$ nanocomposites.

3.3. ANN Modeling and Prediction

In general, if the R^2 value is larger and MSE is lower, the optimal model is better. A data set of 29 rows were employed to develop the ANN structure and the ANN training was estimated by the gradient descent method. The coefficient of determination of the developed ANN model for the Sb(III) removal by the $\text{Fe}_3\text{O}_4/\text{GO}$ nanocomposites was approximately 0.9939 (Figure S5). The epoch was set as 2,000, the learning rate was designed at 0.1, the goal was set as $1e^{-5}$, and momentum factor was set as 0.9. As demonstrated in Figure S6, the ANN training was stopped after the epoch reached 573 with the lowest MSE ($1e^{-3.21}$). The different numbers of neurons (1 ~ 10) in hidden layer were employed to determine the best structure of ANN model for Sb(III) removal from aqueous solutions based on the maximum R^2 value and the lowest MSE value in the present study (Table S5). The larger number of hidden layer neurons is good for training, yet it is not conducive to model performance because they may cause the over-fitting of trained network. The phenomenon of the network generalization disability would happen under a large number of hidden layer nodes. The hidden layer with 3 neurons is the most suitable architecture for the Sb(III) removal process (Figures S7 and S8).

ANN-GA was employed to obtain the global optimum by fast search in the whole solution space. The values of the operating parameters for GA were set to be: population size = 20, crossover probability = 0.8 and mutation probability = 0.01. The GA was done for 100 generations to achieve the maximum removal efficiency by optimizing the four factors. The predicted

Table 1. ANOVA for Response Surface Quadratic Model

Source	Sum of squares	Degree of freedom	Mean square	F value	p value	
Model	1,540.03	14	110.00	5.00	0.0024	significant
A	0.89	1	0.89	0.04	0.8436	
B	39.77	1	39.77	1.81	0.2000	
C	1.59	1	1.59	0.07	0.7918	
D	1.47	1	1.47	0.07	0.8000	
AB	13.14	1	13.14	0.60	0.4523	
AC	18.75	1	18.75	0.85	0.3714	
AD	112.68	1	112.68	5.13	0.0400	
BC	138.77	1	138.77	6.31	0.0249	
BD	7.26	1	7.26	0.33	0.5746	
CD	0.56	1	0.56	0.03	0.8760	
A ²	613.8	1	613.80	27.92	0.0001	
B ²	4.83	1	4.83	0.22	0.6466	
C ²	15.66	1	15.66	0.71	0.4128	
D ²	9.21	1	9.21	0.42	0.5280	
Residual	307.79	14	21.99			
Lack of fit	278.43	10	27.84	3.79	0.1053	not significant
Pure error	29.36	4	7.34			
Corrected total	1,847.83	28				

Note: $R^2 = 0.8334$, Adj. $R^2 = 0.6669$, Adequate Precision = 9.032 and CV = 6.17%

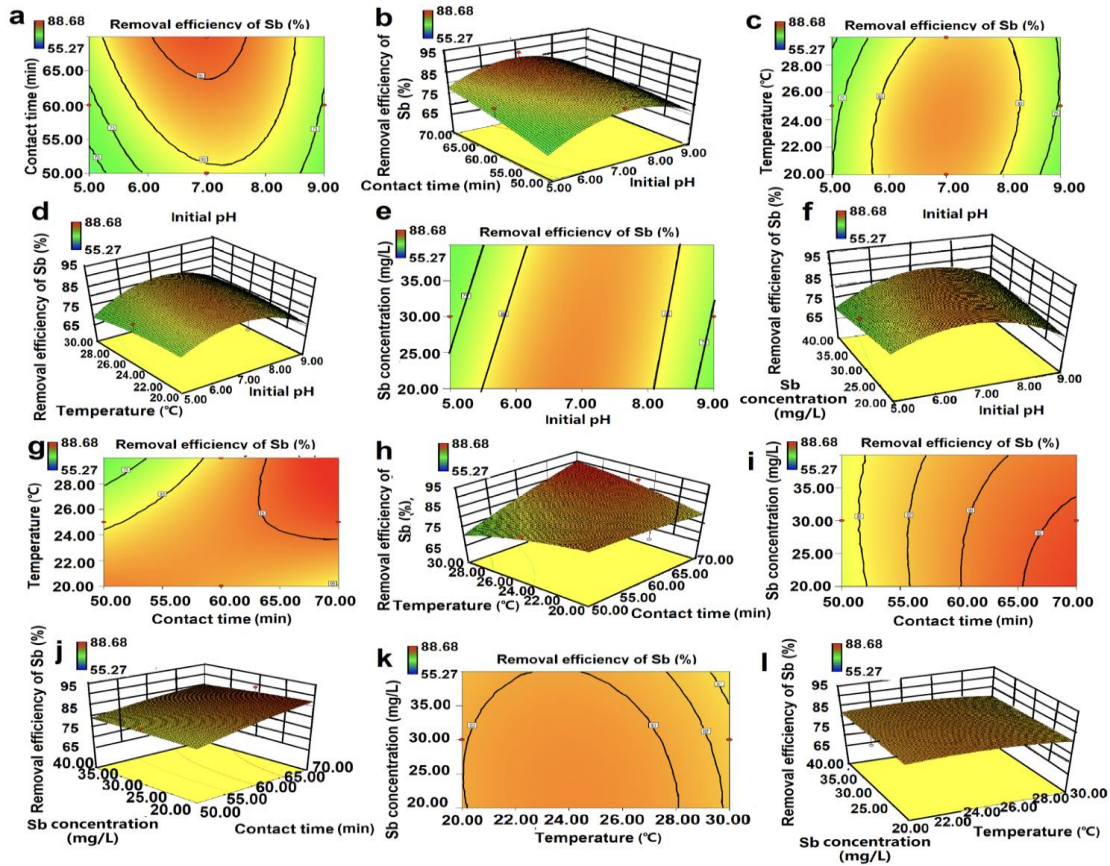


Figure 7. (a) Contour and (b) 3-D surface plots for interactive effect of contact time and initial pH; (c) contour and (d) 3-D surface plots for interactive effect of temperature and initial pH; (e) contour and (f) 3-D surface plots for interactive effect of initial Sb(III) concentration and initial pH; (g) contour and (h) 3-D surface plots for interactive effect of temperature and contact time; (i) contour and (j) 3-D surface plots for interactive effect of initial Sb(III) concentration and contact time; (k) contour and (l) 3-D surface plots for interactive effect of initial Sb(III) concentration and temperature on the removal of the Sb(III).

maximum removal efficiency of Sb(III) by Fe₃O₄/GO nanocomposites was approximately 94.75% under the following conditions: temperature = 24.96 °C, initial pH = 5.83, initial Sb(III) concentration = 39.69 mg/L and contact time = 64.92 min (Figure 8). The removal efficiency for the confirmatory experiment was 92.41%, and the absolute error was 2.34% compared with the predictive value. It is thus shown that the model is reliable for predicting the Sb(III) removal using the Fe₃O₄/GO nanocomposites.

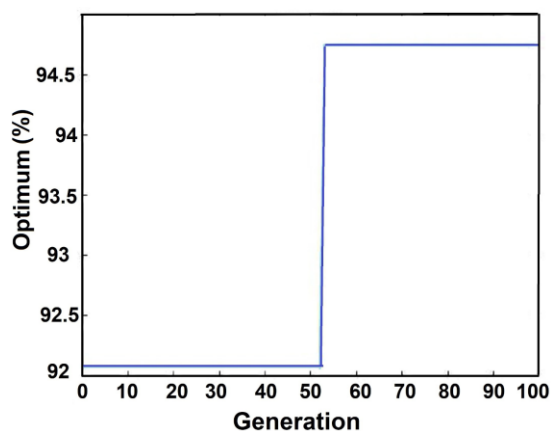


Figure 8. Evolution of fitness with 100 generations.

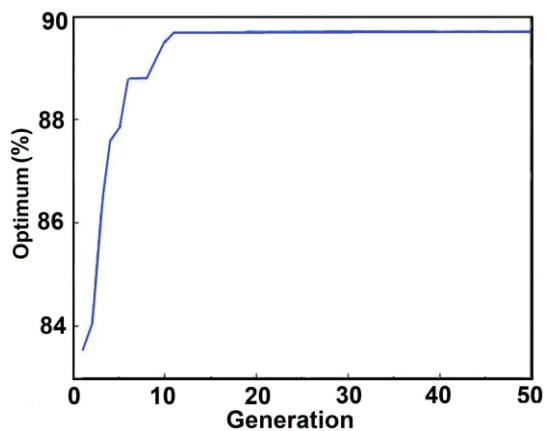


Figure 9. The maximum removal efficiency against iterations.

A hybrid ANN-PSO model was also employed to predict maximum removal of Sb(III) from aqueous solutions in this study. The swarm size, maximum iteration, c_1 , c_2 , minimum inertia weight and maximum inertia weight were 20, 50, 2, 2, 0.3, and 0.9, respectively. Optimal conditions were selected after the evaluation of ANN-PSO for approximately 10 iterations to achieve the maximum removal efficiency of Sb(III) (Figure 9). The predicted maximum removal efficiency of Sb(III) from aqueous solutions using ANN-PSO is 89.72% under the following conditions: temperature = 22.14 °C, initial pH = 8.06, initial Sb(III) concentration = 53.89 mg/L and contact time = 56.04 min. The removal efficiency for the confirmatory experiments was 85.16%, and the absolute error was 4.52% in comparison with the predicted value.

3.4. Comparison of Different Models

The different models, i.e., RSM, ANN-GA, and ANN-PSO models, for Sb(III) removal from aqueous solutions by Fe₃O₄/GO nanocomposites were compared to obtain the best one. Firstly, the R^2 value of the ANN model is obviously higher than that of RSM model (Table 2). Then, the MSE value of ANN-GA model is less than that of the ANN-PSO and RSM models. This means that the ANN-GA model was a suitable model for predicting the Sb(III) removal from aqueous solutions by Fe₃O₄/GO nanocomposites.

Table 2. The Optimized Process Parameters for Sb(III) Removal by Fe₃O₄/GO Nanocomposites Using Different Approaches

Process parameters	Optimization		
	ANN-GA	ANN-PSO	RSM
Operating temperature (°C)	24.96	22.14	30
Initial pH	5.83	6.78	7.06
Initial Sb(III) concentration (mg/L)	39.69	30	30
Contact time (min)	64.92	60.00	70
Removal efficiency of model (%)	94.75%	89.72%	90.12%
Experimental verification values (%)	92.41%	85.16%	86.22%
Average values of absolute errors (%)	2.34%	4.56%	3.90%
R^2	0.9949		0.8334
MSE	0.0028		0.03176

RSM is a statistical method that uses reasonable experimental design method and gets certain data through experiments, uses multiple quadratic regression equation to fit the functional relationship between factors and response values, and seeks the optimal process parameters through the analysis of regression equation to solve multivariable problems (Kola et al., 2017). However, RSM is prone to fall into a local optimum. ANN has slow convergence speed and also easy to fall into local optimum (Wong et al., 2006). PSO has the ability of expanding search space and fast convergence speed, which also falls into a local optimum for complex problems because of the lack of local search (Pratiwi et al., 2011). GA has good global searching ability, which can search all the solutions in the solution space quickly without falling into the trap of fast descent of the local optimal solution (Das et al., 2013). Moreover, the distributed computing can be carried out conveniently and the solving speed can be accelerated by using its inherent parallelism. However, the local search ability of genetic algorithm is poor, which makes the simple genetic algorithm time-consuming and inefficient in the later evolution stage. Therefore, ANN-GA has the characteristics of full optimum search and fast search. Particles in PSO share information only by searching for the best point at present. In fact, it is a single-item information sharing mechanism. In GA, chromosomes share information with each other, which makes the whole population move to the optimal region. In addition, GA can be used to study three aspects of ANN (network connec-

tion weight, network structure, and learning algorithm). The advantage is that GA can deal with several problems, i.e., non-differentiable node transfer function or no gradient information. Hence, compared with the RSM and ANN-PSO model, the ANN-GA model was a more suitable model in this study.

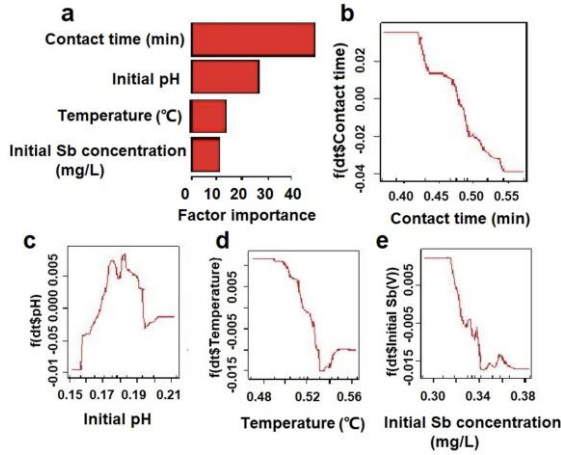


Figure 10. Feature importance for GBRT.

Table 3. Comparison among F Value, GBRT and Garson Methods of Factors Importance

Factors	GBRT		F test		Garson	
	Relative influence (%)	Order	F value	Order	Relative important (%)	Order
Contact time	48.74	1	1.18	1	36.69	1
pH	26.72	2	0.04	4	31.27	2
Temperature	13.70	3	0.072	2	25.31	4
Initial concentration	10.84	4	0.067	3	6.73	3

Feature interpretation is one of the advantages of GBRT models. It is possible to rank features according to their contribution to the model performance. Features frequently used for splitting branches of the regression trees causing a reduction in training error are ranked better than features not being used for splitting (Persson et al, 2017). By tracking the splits and the associated reduction in training error during the model fit, the features can be ranked according to their importance in the model. As shown in Figure 10, the features are sorted such that the most important feature appears on top of the bar plots. F value, GBRT and Garson method all demonstrates that contact time is the most influential variable for Sb(III) removal (Table 3).

3.5. Adsorption Equilibrium Study

The equilibrium data were fitted to Langmuir, Freundlich and Temkin isotherms and the results for their parameters are shown in Table 4 and Figure S9. In this study, the best suitable isotherm model for Sb(III) removal from aqueous solutions by the nanocomposites was the linear-Langmuir isotherm model due to the higher value of R^2 and lower value of χ^2 , SAE and APE than those of Freundlich and Temkin isotherm models.

Therefore, the adsorption process was controlled by the monolayer adsorption on a homogeneous surface. In addition, the R_L values calculated for Langmuir isotherm is exhibited in Table S6, which lie in the range of 0.0254 ~ 0.5659. It was suggested that the adsorption of Sb(III) onto the Fe_3O_4/GO nanocomposites is a favorable adsorption. Further, lower R_L values at higher initial Sb(III) concentration show that the adsorption was more favorable at a higher concentration (Figure S10). The degree of favorability was generally related to the irreversibility of the system. The maximum adsorption quantity for the nanocomposites in this study is 34.48 mg/kg, which is higher than that of other materials shown in Table 5. For the Freundlich isotherm model, the value of n in the range 2 ~ 10, 1 ~ 2, and less than 1 stands for a good, moderately difficult, and poor adsorption, respectively (Asl et al., 2013). The n values obtained from linear and non-linear fittings for the Freundlich isotherm model were 3.6245 and 1.5934 in this study, respectively. The n value obtained from linear fitting to the Freundlich isotherm model shows a good adsorption of Sb(III) onto the nanocomposites. Based on R^2 value, Chi-square, APE and SAE, the best suitable isotherm model of the adsorption process obeys the following order: Langmuir model > Freundlich model > Temkin model (Figure S9).

3.6. Kinetics Study

Adsorption kinetics is important for the evaluation of adsorption process. The pseudo-first-order kinetic, pseudo-second-order kinetic and intraparticle diffusion models were used to investigate the Sb(III) adsorption onto Fe_3O_4/GO nanocomposites from the solutions, which can be calculated using the following Equations (7) ~ (9) (Ho and McKay, 1998; Ho, 2004; Fan et al., 2014):

$$\ln(q_e - q_t) = \ln q_e - k_1 t \tag{7}$$

$$\frac{t}{q_t} = \frac{1}{k_2 q_e^2} + \frac{t}{q_e} \tag{8}$$

$$q_t = k_d t^{0.5} + C \tag{9}$$

where q_e and q_t are the adsorption capacity (mg/g) at equilibrium and time t , respectively; k_1 (1/min) is the rate constant of pseudo-first-order adsorption reaction; k_2 is the rate constant for the pseudo-second-order adsorption reaction (g/mg·min); k_d is the intraparticle diffusion rate constant (mg/g·min^{0.5}) and C is the intercept for the equation. Based on the R^2 value (Table 6), pseudo-second-order model is the better kinetic model to describe the adsorption of Sb(III) onto Fe_3O_4/GO nanocomposites than the pseudo-first-order and intraparticle diffusion models (Figure S11). On the basis of these results, it can be summarized that the pseudo-second-order model is suitable for describing the kinetic behavior of the adsorption.

3.7. Thermodynamic Parameters

The adsorption thermodynamics can provide key information to evaluate spontaneous or exothermic nature of a removal

Table 4. The Langmuir, Freundlich and Temkin Isotherm Parameters for Sb(III) Adsorption on The Fe₃O₄/GO Nanocomposites

Isotherms	Parameters	Value of parameters obtained by the linear fitting	Value of parameters obtained by the nonlinear fitting
Langmuir	k (L/mg)	0.7672	0.3180
	q_m (mg/g)	34.4800	42.4200
	R^2	0.9974	0.9780
	x^2	0.5910	1.7323
	APE(%)	6.9439	11.8502
	SAE	6.8102	10.4609
Freundlich	k_F (mg/g)	15.4236	6.5670
	$1/n$	0.2759	0.6276
	R^2	0.8681	0.8681
	x^2	0.6664	2.0590
	APE(%)	11.6604	51.4753
	SAE	13.8890	43.6650
Temkin	A	15.0850	
	B	15.1220	
	R^2	0.8585	
	APE(%)	8.2984	
	x^2	1.0695	
	SAE	9.6243	

process with different temperatures, which can be calculated using the following Equations (10) ~ (12) (Wu et al., 2009; Cao et al., 2017):

$$\ln K_T = \frac{\Delta S^0}{R} - \frac{\Delta H^0}{RT} \quad (10)$$

$$\Delta G^0 = -RT \ln K_T \quad (11)$$

$$K_T = \frac{C_0}{C_e} \quad (12)$$

where ΔH^0 and ΔS^0 are the standard enthalpy change (kJ mol⁻¹ K⁻¹) and the standard entropy change (kJ mol⁻¹ K⁻¹), which can be obtained from the slope and intercept of a plot of $\ln K_0$ against $1/T$, respectively; ΔG^0 is the standard free energy change (kJ/mol); T is the temperature (K); R is gas constant (8.314 J mol⁻¹ K⁻¹).

The effect of temperature on the adsorption process of Sb(III) by the Fe₃O₄/GO nanocomposites was estimated at 293, 298, 303, and 313 K, respectively. The calculated value of Gibbs free energy (ΔG^0), enthalpy change (ΔH^0) and entropy change (ΔS^0), are shown in Table 7. The value of ΔG^0 was calculated as -2.6335, -3.2195, -3.4151, and 4.3049 kJ mol⁻¹ for 293, 298, 303, 313, and 323 K, respectively. The decrease in ΔG^0 values with the increasing temperature means that the sorption reaction was spontaneous. The positive value obtained of the ΔH^0 in this study indicates the endothermic nature of the Sb(III) adsorption onto the Fe₃O₄/GO nanocomposites, which demonstrated that the process consumes energy. The positive value of ΔS^0 showed the increasing randomness at the solid/liquid interface during sorption of Fe₃O₄/GO. Therefore, the positive values of both ΔH^0 and ΔS^0 exhibited that the adsorption process was

entropy-driven.

Table 5. The Maximum Adsorption Capacity of Sb(III) for Different Materials

Sorbent	Sorption capacity (mg/kg)	Reference
Cyanobacteria microcystis biomass	4.8800	(Wu et al. 2012)
Montmorillonite	11.6100	(Anjum and Datta, 2012)
Imprinted polymer	6.7000	(Fan et al. 2013)
Sb(III)-imprinted sorbent	27.7000	(Mendil et al. 2013)
Sb(III)-imprinted silica gel	32.4000	(Fan et al. 2014)
Bentonite	0.3700	(Xi et al. 2011)
Graphene	7.5000	(Leng et al. 2012)
Fe ₃ O ₄ /GO nanocomposites	34.4800	In this study

Table 6. Kinetic Parameters for Sb(III) Removal by The Fe₃O₄/GO Nanocomposites

Model	Parameters	Value of parameters
Pseudo-first-order	k_1 (min ⁻¹)	0.1912
	R^2	0.8701
	q_e	27.6929
Pseudo-second-order	k_2 (g·mg ⁻¹ ·min ⁻¹)	0.0107
	R^2	0.994
	q_e	26.3852
Intraparticle diffusion	k_3 (mg·g ⁻¹ ·min ^{-1/2})	0.9931
	B (mg·g ⁻¹)	16.584
	R^2	0.8898

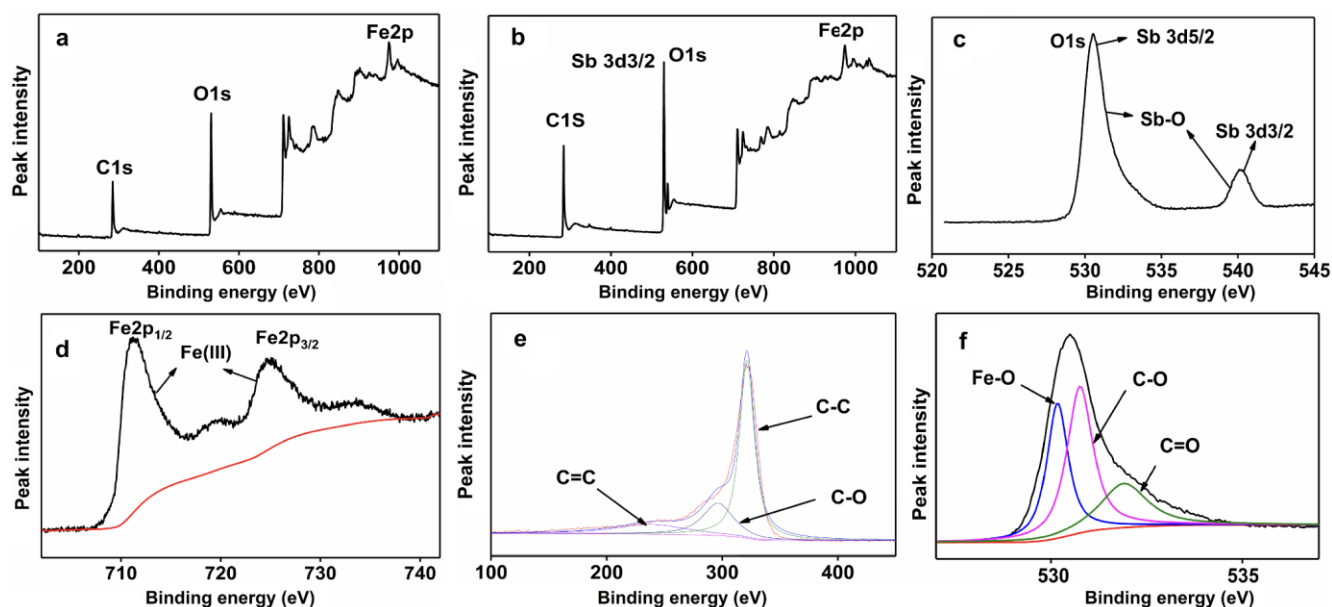


Figure 11. XPS spectrum of $\text{Fe}_3\text{O}_4/\text{GO}$ nanocomposites (a) before and (b) after the adsorption of Sb(III) ; (c) the high-resolution XPS spectrum of $\text{Sb}_{5/2}$, $\text{Sb}_{3/2}$ and O_{1s} ; (d) the high-resolution spectrum of Fe_{2p} ; (e) C_{1s} XPS spectrum of the $\text{Fe}_3\text{O}_4/\text{GO}$ composites; (f) O_{1s} XPS spectrum of the $\text{Fe}_3\text{O}_4/\text{GO}$ composites.

Table 7. Thermodynamic Parameters for Sb(III) Removal by $\text{Fe}_3\text{O}_4/\text{GO}$ Nanocomposites

ΔH^0 ($\text{kJ}\cdot\text{mol}^{-1}$)	ΔS^0 ($\text{J}\cdot\text{mol}^{-1}\text{K}^{-1}$)	ΔG^0 (kJ/mol)			
		293 K	298 K	303 K	313 K
20.8781	80.4363	-2.6335	-3.2195	-3.4151	-4.3049

3.8. Analysis of Adsorption Mechanism

The XPS spectra of $\text{Fe}_3\text{O}_4/\text{GO}$ before and after the adsorption of Sb(III) were used to analyze the adsorption mechanism. It was observed that the peaks of Sb and O_{1s} exist after the adsorption of Sb(III) onto $\text{Fe}_3\text{O}_4/\text{GO}$ (Figure 11a). The values (540.04 and 530.52 eV) of binding energy for $\text{Sb } 3d$ were for $\text{Sb } (3d_{5/2})$ and $\text{Sb } (3d_{3/2})$, respectively (Figure 11b). It was illustrated that Sb_2O_5 as the pentavalent antimony existed on the $\text{Fe}_3\text{O}_4/\text{GO}$ according to the XPS chemical state database (Yang et al., 2017). However, the antimony of $\text{K}(\text{SbO})\text{C}_4\text{H}_4\text{O}_6 \cdot 1/2$ as the stock solutions was a trivalent species in this study. Thus, it can be confirmed that the redox reaction existed in the reaction process because Sb(III) was oxidized to Sb(V) . This means that the hazard of Sb was decreased using the nanocomposites in water environment. In addition, the presence of $\text{Fe } (2p_{1/2})$, $\text{Fe } (2p_{3/2})$, C-C , C=O , C-O , Fe-O , and C=C are shown in Figures 11c ~ 11f, which further proved that the Fe_3O_4 nanoparticles were successfully supported on GO sheet.

3.9. Regeneration of the $\text{Fe}_3\text{O}_4/\text{GO}$ Nanocomposites

The regeneration of the adsorbent is an important factor in assessing its possibility for practical applications. The adsorption cycles of Sb(III) were repeated thrice using eluent of 0.1 mol/L HCl and the Sb(III) -loaded $\text{Fe}_3\text{O}_4/\text{GO}$ composites were separat-

ed by a permanent magnet. As shown in Figure 12, the removal efficiencies of the first regeneration cycle, second regeneration cycle, third regeneration cycle and fourth regeneration cycle are 93.44, 89.16, 81.86, and 75.93%, respectively. The result reveals that the gradual decline in the adsorption capacity of $\text{Fe}_3\text{O}_4/\text{GO}$ nanocomposites for Sb(III) occurred for four consecutive adsorption cycles and the dramatic decline was observed after four regeneration cycles, indicating that $\text{Fe}_3\text{O}_4/\text{GO}$ nanocomposites are an effective and reusable adsorbent.

4. Conclusion

According to the results of XRD, SEM, TEM, XPS, FT-IR, N_2 -sorption, and SQUID, the mesoporous $\text{Fe}_3\text{O}_4/\text{GO}$ nanocomposites were controllably synthesized in this work. Fe_3O_4 nanoparticles with the average size of 30.04 nm were uniformly distributed on the surface of GO sheets. The successful in-situ growth of the nanoparticles was ascribed to the oxygen-containing groups of GO. The pore size distribution of these is narrow and centered at 3.65 nm. The maximum Sb(III) removal efficiency predicted was 94.75% using ANN-GA model under the optimal conditions (temperature = 24.96 °C, initial pH = 5.83, initial Sb(III) concentration = 39.69 mg/L, and contact time = 64.92 min). Analysis of variance, GBRT and Garson method exhibited that contact time appears to be the most influential variable for the Sb(III) removal. The fitting results show that the Langmuir isotherm and pseudo-second-order kinetic model could satisfactorily describe the adsorption process, which was spontaneous and entropy-driven. The mechanism study on the removal of Sb(III) demonstrated that the adsorption process was accompanied with redox reaction. The regeneration experiments showed that $\text{Fe}_3\text{O}_4/\text{GO}$ nanocomposites are an effective and reusable ad-

sorbent within four regeneration cycles.

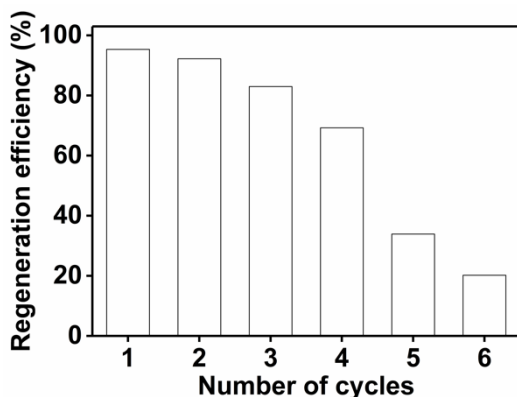


Figure 12. Evolution of regeneration efficiency after each regeneration cycle ($\text{Fe}_3\text{O}_4/\text{GO}$ nanocomposites dosage = 20 mg; temperature = 25 °C; contact time = 60 min; initial Sb(III) concentration = 30 mg/L; initial pH = 7).

In order to further explore the mechanism of the adsorption process, X-ray absorption near edge structure (XANES) analysis based on synchrotron radiation can be used to identify the local atomic environment (i.e., valence, coordination) of metals after the adsorption of Sb onto $\text{Fe}_3\text{O}_4/\text{GO}$. When high-energy particles including electrons are in acceleration and forced to travel in a curved path by a magnetic field, synchrotron radiation is produced. Small angle X-ray diffraction analysis can also be used to obtain information concerning the state (e.g., mesopores) of the samples in the nanometer length scale. Additionally, the size of nanoparticles will be decreased with the drop of the apparent activation energy and the growth of the reaction rate in the heterogeneous systems. Therefore, it is of great significance to study how to further reduce the size of nanoparticles to accelerate the reaction. Finally, a scale up system (e.g. permeable reactive barrier) needs to be used for Sb(III) removal with the aid of more advanced AI techniques.

Acknowledgments. This research was financially supported by the National Natural Science Foundation of China (Grant No. 21667012), the Government of Guizhou Province (Project No. [2017] 5726-42) and the National 111 Project of China (Grant No. D17016).

References

- Abdollahi, Y., Zakaria, A., Abbasiyannejad, M., Masoumi, H.R.F., Moghaddam, M.G., Matori, K.A., Jahangirian, H. and Keshavarzi, A. (2013). Artificial neural network modeling of p-cresol photodegradation. *Chem. Cent. J.* 7(1), 96. <https://doi.org/10.1186/1752-153X-7-96>
- Alothman, Z. (2012). A review: Fundamental aspects of silicate mesoporous materials. *Materials*. 5(12), 2874-2902. <https://doi.org/10.3390/ma5122874>
- Anjum, A. and Datta, M. (2012). Adsorptive removal of antimony (III) using modified montmorillonite: A study on sorption kinetics. *J. Anal. Sci., Methods Instrum.* 2(3), 167-175. <https://doi.org/10.4236/jasmi.2012.23027>
- Asl, S.H., Ahmadi, M., Ghiasvand, M., Tardast, A. and Katal, R. (2013). Artificial neural network (ANN) approach for modeling of Cr(VI) adsorption from aqueous solution by zeolite prepared from raw fly ash (ZFA). *J. Ind. Eng. Chem.* 19, 1044-1055. <https://doi.org/10.1016/j.jiec.2012.12.001>
- Behnam, A.L., Nader, K.M. and Mohammad, R.M. (2019). Phytoextraction of heavy metals from contaminated soil, water and atmosphere using ornamental plants: mechanisms and efficiency improvement strategies. *Environ. Sci. Pollut. R.* 26, 8468-8484. <https://doi.org/10.1007/s11356-019-04241-y>
- Cao, R.S., Fan, M.Y., Hu, J.W., Ruan, W.Q., Xiong, K.N. and Wei, X.H. (2017). Optimizing low-concentration mercury removal from aqueous solutions by reduced graphene oxide-supported Fe_3O_4 composites with the aid of an artificial neural network and genetic algorithm. *Materials*. 10(11), 1279. <https://doi.org/10.3390/ma10111279>
- Chang, Y.H., Li, J., Wang, B., Luo, H. and Zhi, L.J. (2014). A facile synthetic approach to reduced graphene oxide- Fe_3O_4 composite as high performance anode for lithium-ion batteries. *J. Mater. Sci. Technol.* 30, 759-764. <https://doi.org/10.1016/j.jmst.2014.01.010>
- Chaves, L.L., Vieira, A.C.C., Ferreira, D., Sarmento, B. and Reis, S. (2015). Rational and precise development of amorphous polymeric systems with dapsone by response surface methodology. *Int. J. Biol. Macromol.* 81, 662-671. <https://doi.org/10.1016/j.ijb.2015.08.009>
- Chen, X.L., Fu, J.P., Yao, J.L. and Gan, J.F. (2017). Prediction of shear strength for squat RC walls using a hybrid ANN-PSO model. *Eng. Comput.* 34, 367-383. <https://doi.org/10.1007/s00366-017-0547-5>
- Chen, C., Cheng, T., Shi, Y.S. and Tian, Y. (2014a). Adsorption of Cu(II) from aqueous solution on fly ash based linde F(K) Zeolite, Iran. *J. Chem. Chem. Eng.* 33, 29-35. <https://doi.org/10.30492/IJCCE.2014.11328>
- Chen, C., Cheng, T., Wang, Z.L. and Han, C.H. (2014b). Removal of Zn^{2+} in aqueous solution by Linde F(K) zeolite prepared from recycled fly ash. *J. Indian Chem. Soc.* 91, 1-7. <https://doi.org/10.5281/zenodo.5749139>
- Chen, C., Cheng, T., Zhang, X., Wu, R.X. and Wang, Q.Y. (2019). Synthesis of an efficient Pb adsorption nano-crystal under strong alkali hydrothermal environment using a gemini surfactant as directing agent. *J. Chem. Soc. Pak.* 41(6), 1034-1038. <https://doi.org/10.52556/000821/JCSP/41.06.2019>
- Cheng, T., Chen, C., Tang, R., Han, C.H. and Tian, Y. (2018). Competitive adsorption of Cu, Ni, Pb, and Cd from aqueous solution onto fly ash-based Linde F(K) zeolite. *Iran. J. Chem. Chem. Eng.* 37(1), 61-72. <https://doi.org/10.30492/IJCCE.2018.31971>
- Chung, T.F., Shen, T., Cao, H.L., Jauregui, L.A., Wu, W., Yu, Q.K., Newell, D. and Chen, Y.P. (2013). Synthetic graphene grown by chemical vapor deposition on copper foils. *Int. J. Mod. Phys. B.* 27, 1341002. <https://doi.org/10.1142/s0217979213410026>
- Das, S. and Mishra, S. (2017). Box-Behnken statistical design to optimize preparation of activated carbon from Limonia acidissima shell with desirability approach. *J. Environ. Chem. Eng.* 5(1), 588-600. <https://doi.org/10.1016/j.jece.2016.12.034>
- Dong, G.H., Huang, L.H., Xu, X.Y., Wang, C., Liu, Y.Y., Liu, G.F., Wang, L., Liu, X.W. and Xia, H.B. (2013). Effect and mechanism analysis of MnO_2 on permeable reactive barrier (PRB) system for the removal of tetracycline. *Chemosphere*. 193, 702-710. <https://doi.org/10.1016/j.chemosphere.2017.11.085>
- Fan, H.T., Liu, J.X., Yao, H., Zhang, Z.G., Yan, F. and Li, W.X. (2013). Ionic imprinted silica-supported hybrid sorbent with an anchored chelating schiff base for selective removal of Cadmium(II) ions from aqueous media. *Ind. Eng. Chem. Res.* 53, 369-378. <https://doi.org/10.1021/ie4027814>
- Fan, H.T., Sun, Y., Tang, Q., Li, W.L. and Sun, T. (2014). Selective adsorption of antimony(III) from aqueous solution by ion-imprinted organic-inorganic hybrid sorbent: Kinetics, isotherms and ther-

- modynamics. *J. Taiwan Inst. Chem. E.* 45, 2640-2648. <https://doi.org/10.1016/j.jtice.2014.07.008>
- Fan, M.Y., Li, T.J., Hu, J.W., Cao, R.S., Shi, X.D. and Ruan, W.Q. (2017). Artificial neural network modeling and genetic algorithm optimization for cadmium removal from aqueous solutions by reduced graphene oxide-supported nanoscale Zero-Valent iron (nZVI/rGO) composites. *Materials*. 10, 544. <https://doi.org/10.3390/ma10050544>
- Fan, M.Y., Hu, J.W., Cao, R.S., Ruan, W.Q. and Wei, X.H. (2018). A review on experimental design for pollutants removal in water treatment with the aid of artificial intelligence. *Chemosphere*. 200, 330-343. <https://doi.org/10.1016/j.chemosphere.2018.02.111>
- Filella, M., Belzile, N. and Lett, M.C. (2007). Antimony in the environment: A review focused on natural waters. III. Microbiota relevant interactions. *Earth-Sci. Rev.* 80, 195-217. <https://doi.org/10.1016/j.earscirev.2006.09.003>
- Guo, L.Q., Ye, P.R., Wang, J., Fu, F.F. and Wu, Z.J. (2015). Three-dimensional Fe₃O₄-graphene macroscopic composites for arsenic and arsenate removal. *J. Hazard. Mater.* 298, 28-35. <https://doi.org/10.1016/j.jhazmat.2015.05.011>
- Guo, X.J., Wu, Z.J. and He, M.C. (2009). Removal of antimony(V) and antimony(III) from drinking water by coagulation-flocculation-sedimentation (CFS). *Water Res.* 43, 4327-4335. <https://doi.org/10.1016/j.watres.2009.06.033>
- Hanrahan, G., Garza, C., Garcia E. and Miller, K. (2007). Experimental design and response surface modeling: a method development application for the determination of reduced inorganic species in environmental samples. *J. Environ. Inform.* 9, 71-79. <https://doi.org/10.3808/jei.200700088>
- Ho, Y.S. and McKay, G. (1998). Sorption of dye from aqueous solution by peat. *Chem. Eng. J.* 70(2), 115-124. [https://doi.org/10.1016/S0923-0467\(98\)00076-1](https://doi.org/10.1016/S0923-0467(98)00076-1)
- Ho, Y.S. (2004). Citation review of Lagergren kinetic rate equation on adsorption reactions. *Scientometrics*. 59, 171-177. <https://doi.org/10.1023/B:SCIE.0000013305.99473.cf>
- Jiao, T.F., Liu, Y.Z., Wu, Y.T., Zhang, Q.R., Yan, X.H., Gao, F.M., Bauer, A.J.P., Liu, J.Z., Zeng, T.Y. and Li, B.B. (2015). Facile and scalable preparation of graphene oxide-based magnetic hybrids for fast and highly efficient removal of organic dyes. *Sci Rep.* 5, 12451. <https://doi.org/10.1038/srep12451>
- Kappen, P., Ferrando-Miguel, G., Reichman, S.M., Innes, L., Welter, E. and Pigram P.J. (2017). Antimony leaching and chemical species analyses in an industrial solid waste: Surface and bulk speciation using ToF-SIMS and XANES. *J. Hazard. Mater.* 329, 131-140. <https://doi.org/10.1016/j.jhazmat.2017.01.022>
- Karimi, H. and Ghaedi, M. (2014). Application of artificial neural network and genetic algorithm to modeling and optimization of removal of methylene blue using activated carbon. *J. Ind. Eng. Chem.* 20, 2471-2476. <https://doi.org/10.1016/j.jiec.2013.10.028>
- Kirmizakis, P., Tsamoutsoglou, C., Kayan, B. and Kalderis, D. (2014). Subcritical water treatment of landfill leachate: application of response surface methodology. *J. Environ. Manage.* 146, 9-15. <https://doi.org/10.1016/j.jenvman.2014.04.037>
- Kola, A.K., Mekala, M., Goli, V.R. (2017). Experimental design data for the biosynthesis of citric acid using Central Composite Design method. *Data Brief.* 12, 234-241. <https://doi.org/10.1016/j.dib.2017.03.049>
- Krachler, M., Emons, H. and Zheng, J. (2001). Speciation of antimony for the 21st century: promises and pitfalls. *Trac-Trend. Anal. Chem.* 20(2), 79-90. [https://doi.org/10.1016/S0165-9936\(0\)00065-0](https://doi.org/10.1016/S0165-9936(0)00065-0)
- Leng, Y.Q., Guo, W.L., Su, S.N., Yi, C.L., Xing, L.T. (2012). Removal of antimony(III) from aqueous solution by graphene as an adsorbent. *Chem. Eng. J.* 2012, 211-212, 406-411. <https://doi.org/10.1016/j.cej.2012.09.078>
- Li, L.L., Luo, C.N., Li, X.J., Duan, H.M. and Wang, X.J. (2014). Preparation of magnetic ionic liquid/chitosan/graphene oxide composite and application for water treatment. *Int. J. Biol. Macromol.* 66, 172-178. <https://doi.org/10.1016/j.ijbiomac.2014.02.031>
- Maamoun, I., Eljamal, O., Falyouna, O., Eljamal, R. and Sugihara, Y. (2020). Multi-objective optimization of permeable reactive barrier design for Cr(VI) removal from groundwater. *Ecotox. Environ. Safe.* 200, 110773. <https://doi.org/10.1016/j.ecoenv.2020.110773>
- Mendil, D., Bardak, H., Tuzen, M. and Soylak, M. (2013). Selective speciation of inorganic antimony on tetraethylenepentamine bonded silica gel column and its determination by graphite furnace atomic absorption spectrometry. *Talanta*. 107, 162-166. <https://doi.org/10.1016/j.talanta.2013.01.010>
- Namvari, M. and Namazi, H. (2014). Clicking graphene oxide and Fe₃O₄ nanoparticles together: an efficient adsorbent to remove dyes from aqueous solutions. *Int. J. Environ. Sci. Te.* 11, 1527-1536. <https://doi.org/10.1007/s13762-014-0595-y>
- Navarro, P. and Alguacil, F.J. (2002). Adsorption of antimony and arsenic from a copper electrorefining solution onto activated carbon. *Hydrometallurgy*. 66(1-3), 101-105. [https://doi.org/10.1016/S0304-386X\(02\)00108-1](https://doi.org/10.1016/S0304-386X(02)00108-1)
- Ogiela, M.R. and Tadeusiewicz, R. (2003). Artificial intelligence structural imaging techniques in visual pattern analysis and medical data understanding. *Pattern Recogn.* 36, 2441-2452. [https://doi.org/10.1016/s0031-3203\(03\)00089-x](https://doi.org/10.1016/s0031-3203(03)00089-x)
- Pedrycz, W. and Chen, S.M. (2015). *Information Granularity, Big Data, and Computational Intelligence*. Springer. pp 39-61. <https://doi.org/10.1007/978-3-319-08254-7>
- Persson, C., Bacher, P., Shiga, T. and Madsen, H. (2017). Multi-site solar power forecasting using gradient boosted regression trees. *Sor. Energy.* 150, 423-436. <https://doi.org/10.1016/j.solener.2017.04.066>
- Pratiwi, L., Choo, Y.H. and Muda, A.K. (2011). An empirical study of density and distribution functions for ant swarm optimized rough reducts. *Commun. Comput. Inform. Sci.* 180, 590-604. <https://doi.org/10.1016/j.dib.2017.03.049>
- Qi, T., Huang, C., Yan, S., Li, X.J. and Pan, S.Y. (2015). Synthesis, characterization and adsorption properties of magnetite/reduced graphene oxide nanocomposites. *Talanta*. 144, 1116-1124. <https://doi.org/10.1016/j.talanta.2015.07.089>
- Rakshit, S., Sarkar, D., Punamiya, P. and Datta, R. (2011). Antimony sorption at gibbsite-water interface. *Chemosphere*. 84, 480-483. <https://doi.org/10.1016/j.chemosphere.2011.03.028>
- Ruan, W.Q., Shi, X.D., Hu, J.W., Hou, Y., Fan, M.Y., Cao, R.S. and Wei, X.H. (2018). Modeling of malachite green removal from aqueous solutions by nanoscale zerovalent zinc using artificial neural network. *Appl. Sci.* 8(1), 3. <https://doi.org/10.3390/app8010003>
- Sarı, A., Çıtak, D. and Tuzen, M. (2010). Equilibrium, thermodynamic and kinetic studies on adsorption of Sb(III) from aqueous solution using low-cost natural diatomite. *Chem. Eng. J.* 162(2), 521-527. <https://doi.org/10.1016/j.cej.2010.05.054>
- Satyabrata, S., Kotal, A., Mandal, T.K., Giri, S., Nakamura, H. and Kohara, T.A. (2004). Size-Controlled synthesis of magnetite nanoparticles in the presence of polyelectrolytes. *Journal Biosci. Bioeng.* 16(18), 3489-3496. <https://doi.org/10.1021/cm049205n>
- Shan, C., Ma, Z.Y. and Tong, M.P. (2014). Efficient removal of trace antimony(III) through adsorption by hematite modified magnetic nanoparticles. *J. Hazard. Mater.* 268, 229-236. <https://doi.org/10.1016/j.jhazmat.2014.01.020>
- Shen, Y.F., Tang, J., Nie, Z.H., Wang, Y.D., Ren, Y. and Zuo, L. (2009). Preparation and application of magnetic Fe₃O₄ nanoparticles for wastewater purification. *Sep. Purif. Technol.* 68, 312-319. <https://doi.org/10.1016/j.seppur.2009.05.020>
- Teo, P.S., Lim, H.N., Huang, N.M., Chia, C.H. and Harrison, I. (2012). Room temperature in situ chemical synthesis of Fe₃O₄/graphene. *Ceram. Int.* 38(8), 6411-6416. <https://doi.org/10.1016/j.ceramint.2012.05.014>
- Thirugnanasambandham, K. and Sivakumar, V. (2015). Enzymatic catalysis treatment method of meat industry wastewater using lacasse.

- J. Environ. Health Sci.* 13, 86. <https://doi.org/10.1186/s40201-015-0239-2>
- Toushmalani, R. (2013). Gravity inversion of a fault by Particle swarm optimization (PSO). *Springerplus*. 2, 1-7. <https://doi.org/10.1186/2193-1801-2-315>
- Vimlesh, C., Park, J., Chun, Y., Lee, J.W., Hwang, I.C. and Kwang S.K. (2010). Water-dispersible magnetite-reduced graphene oxide composites for arsenic removal. *Acs Nano*. 4, 3985-3979. <https://doi.org/10.1021/nn1008897>
- Wang, Z.H., Gong, D.Y., Li, X., Li, G.T. and Zhang, D.H. (2017). Prediction of bending force in the hot strip rolling process using artificial neural network and genetic algorithm (ANN-GA). *Inter. J Adv. Manuf. Tech.* 93, 3325-3338. <https://doi.org/10.1007/s00170-017-0711-5>
- Watkins, R., Weiss, D., Dubbin, W., Peel, K., Coles, B. and Arnold, T. (2006). Investigations into the kinetics and thermodynamics of Sb(III) adsorption on goethite (alpha-FeOOH). *J Colloid Interf. Sci.* 303(2), 639-646. <https://doi.org/10.1016/j.jcis.2006.08.044>
- Wong, W.T. and Hsu, S.H. (2006). Application of SVM and ANN for image retrieval. *Eur. J. Oper. Res.* 173(3), 938-950. <https://doi.org/10.1016/j.ejor.2005.08.002>
- Wu, F.C., Sun, F.H., Wu, S., Yan, Y.B. and Xing, B.S. (2012). Removal of antimony(III) from aqueous solution by freshwater cyanobacteria *Microcystis* biomass. *Chem. Eng. J.* 183, 172-179. <https://doi.org/10.1016/j.cej.2011.12.050>
- Wu, F.C., Tseng, R.L. and Juang, R.S. (2009). Initial behavior of intraparticle diffusion model used in the description of adsorption kinetics. *Chem. Eng. J.* 153(1-3), 1-8. <https://doi.org/10.1016/j.cej.2009.04.042>
- Xi, J.H., He, M.C. and Lin, C.Y. (2011). Adsorption of antimony(III) and antimony(V) on bentonite: Kinetics, thermodynamics and anion competition. *Microchem. J.* 97(1), 85-91. <https://doi.org/10.1016/j.microc.2010.05.017>
- Yang, X.Z., Zhou, T.Z., Ren, B.Z., Shi, Z. and Hursthouse, A. (2017). Synthesis, characterization, and adsorptive properties of Fe₃O₄/GO nanocomposites for antimony removal. *J. Anal. Methods Chem.* 2017, 3012364. <https://doi.org/10.1155/2017/3012364>
- Zhang, X.Y., Zhou, J.Y., Fu, W., Li, Z.D., Zhong, J., Yang, J.L., Xiao L. and Tan, H. (2010). Response surface methodology used for statistical optimization of jeans-peptide production by *Bacillus subtilis*. *Electron. J. Biotechnol.* 13(4), 6-7. <https://doi.org/10.2225/vol13-issue4-fulltext-5>
- Zhang, Y., and Pan, B. C. (2014). Modeling batch and column phosphate removal by hydrated ferric oxide-based nanocomposite using response surface methodology and artificial neural network. *Chem. Eng. J.*, 249, 111-120. <https://doi:10.1016/j.cej.2014.03.073>
- Zhou, Y.C., Gu, T.F., Yi, W.T., Zhang, T.Q. and Zhang, Y.P. (2019). The release mechanism of heavy metals from lab-scale vertical flow constructed wetlands treating road runoff. *Environ. Sci. Pollut. R.* 26, 16588-16595. <https://doi.org/10.1007/s11356-019-05097-y>
- Zhu, L.Y., Zeng, X.J., Li, X.P., Yang, B. and Yu, R.H. (2017). Hydrothermal synthesis of magnetic Fe₃O₄/graphene composites with good electromagnetic microwave absorbing performances. *J. Magn. Magn. Mater.* 426, 114-120. <https://doi.org/10.1016/j.jmmm.2016.11.063>
- Zong, P.F., Wang, S.F., Zhao, Y.L., Wang, H., Pan, H. and He, C.H. (2013). Synthesis and application of magnetic graphene/iron oxides composite for the removal of U(VI) from aqueous solutions. *Chem. Eng. J.* 220, 45-52. <https://doi.org/10.1016/j.cej.2013.01.038>